Chinese Chemical Letters 37 (2026) 110625

Contents lists available at ScienceDirect

Chinese Chemical Letters

journal homepage: www.elsevier.com/locate/cclet

Amino substitution strategy achieves significant blue shift while preserving high optical anisotropy: $A_2(H_3C_3N_4S_2)_2{\bullet}H_2O$ (A =NH_4, K, Rb, Cs)

Shuang Zhao[a], Fei Jia[a], Kaibei Zhan[b,c], Rui-Xi Wang[b], Pengfei Tan[d], Lin Shen[e], Li-Ming Wu[a,b,*], Ling Chen[a,b,*]

[a] Center for Advanced Materials Research, Beijing Normal University, Zhuhai 519087, China
[b] Beijing Key Laboratory of Energy Conversion and Storage Materials, College of Chemistry, Beijing Normal University, Beijing 100875, China
[c] South China Advanced Institute for Soft Matter Science and Technology, School of Emergent Soft Matter, South China University of Technology, Guangzhou 510640, China
[d] Key Laboratory of Bioinorganic and Synthetic Chemistry of Ministry of Education, School of Chemistry, Sun Yat-sen University, Guangzhou 510006, China
[e] Key Laboratory of Theoretical and Computational Photochemistry of Ministry of Education, College of Chemistry, Beijing Normal University, Beijing 100875, China

ARTICLE INFO

Article history:
Received 5 October 2024
Revised 1 November 2024
Accepted 7 November 2024
Available online 10 November 2024

Keywords:
Amino substitution strategy
Planar π-conjugated group
Optical anisotropy
Birefringence
Ultraviolet crystal

ABSTRACT

The trithiocyanurate, $(H_2C_3N_3S_3)^-$, exhibits a strong optical anisotropy but has a small HOMO-LUMO gap, limiting its application to the higher energy wavelength ranges. Herein, by applying an amino substitution strategy, we report that 2-amino-4,6-dimercapto-*S*-triazine, $(H_3C_3N_4S_2)^-$, generates a series new compound: $A_2(H_2C_3N_4S_2)_2{\bullet}H_2O$ (NH_4, **I**; K−Cs, **II**−**IV**). Compound **I** crystallizes in $P2_1/n$, while compounds **II**–**IV** crystallize in $P\bar{1}$. Their experimental optical band gaps (E_g) range from 3.52 eV to 3.65 eV, corresponding to a blue shift of 30∼60 nm compared to those of the trithiocyanuric containing systems. Moreover, the birefringence of all compounds ranges from 0.440 to 0.510, indicating strong anisotropy. Notably, compound **I** (E_g = 3.65 eV, $\Delta n_{cal.}^{max}$ = 0.510, $\Delta n_{obv.}^{(0\bar{1}\bar{1})}$ = 0.413 at 546 nm) exhibits one of the largest birefringence values among materials with an absorption cutoff edge shorter than 330 nm. The work introduces a new candidate group for preparing optical materials with a desired wide band gap and strong optical anisotropy.

© 2025 Published by Elsevier B.V. on behalf of Chinese Chemical Society and Institute of Materia Medica, Chinese Academy of Medical Sciences.

Birefringence crystals as important optical materials are widely applicated in ultrafast lasers, solid-state lasers, polarizers, phase-matching elements, *etc.* [1–10]. An ideal ultraviolet (UV) or deep-ultraviolet (DUV) nonlinear optical (NLO) crystal must possess a large second-harmonic generation (SHG) response, a wide transparent window and moderate birefringence to achieve phase-matching condition. For a promising UV/DUV birefringent crystal, a wide transparent window and large birefringence also are the key evaluation indicators. Therefore, it is essential to simultaneously enhance both optical anisotropy and optical band gap in the study of UV/DUV optical materials. Previous works show that the π-conjugated group and cations with stereochemically active lone pairs are effective functional structure building units for enhancing the optical anisotropy. However, they do not contribute to the blue shift of absorption cutoff edges according to the "band gap bucket" effect [1]. Therefore, to achieve a balance between optical anisotropy and band gap, the theory of π-conjugated confinement was introduced [2]. Additionally, rational modifications of known structure building units are also an important avenue for discovering new functional materials [3]. The typical inorganic π-conjugated groups $(BO_3)^{3-}$, $(B_3O_6)^{3-}$, $(NO_3)^-$ and $(CO_3)^{2-}$, serve as such building units, and their modified derivatives generate considerable UV/DUV crystals with strong optical anisotropy [4–14].

In additional to inorganic building units, organic groups also offer significant potential, for instance, excellent optical anisotropy [15,16]. The typical units include cyanurate $(H_{3-x}C_3N_3O_3)^{x-}$ (x = 1, 2), trithiocyanurate $(H_{3-x}C_3N_3S_3)^{x-}$, barbiturate $(H_{4-x}C_4N_2O_3)^{x-}$ and melaminate $(H_{6+x}C_3N_6)^{x+}$ are planar π-conjugated groups, similar as $(B_3O_6)^{3-}$, which construct a series of optical crystals [17–23]. Comparing $(H_{3-x}C_6N_7O_3)^{x-}$ (cyamelurate) and $H_3C_3N_3O_3$ (cyanurate), the cyclic oligomerization results in higher polarizability anisotropy, leading to greater birefringence and facilitating the formation of phase-marching crystals [24,25]. However, research on the purposeful structural modification of organic groups to

* Corresponding authors.
E-mail addresses: wlm@bnu.edu.cn (L.-M. Wu), chenl@bnu.edu.cn (L. Chen).

https://doi.org/10.1016/j.cclet.2024.110625
1001-8417/© 2025 Published by Elsevier B.V. on behalf of Chinese Chemical Society and Institute of Materia Medica, Chinese Academy of Medical Sciences.

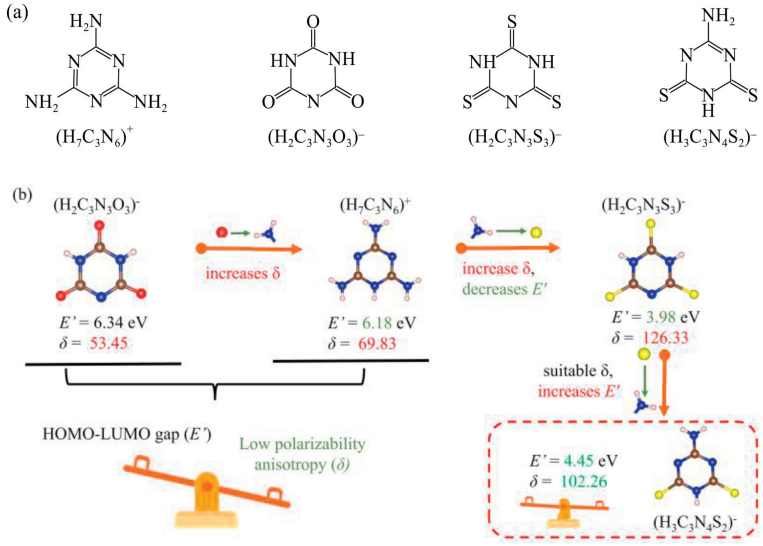


Fig. 1. (a) The structural and molecular formulas of $(H_7C_3N_6)^+$, $(H_2C_3N_3O_3)^-$, $(H_2C_3N_3S_3)^-$ and $(H_3C_3N_4S_2)^-$. (b) A comparison of the HOMO-LUMO gap (*E*') and polarizability anisotropy (δ) for these 6-members ring.

regulate their optical properties is still rare. Rational selection and design are crucial in this context.

As shown in Fig. 1, the highest occupied molecular orbit-lowest unoccupied molecular orbital (HOMO-LUMO) gap (*E*') and polarizability anisotropy (δ) of $(H_2C_3N_3O_3)^-$, $(H_2C_3N_3S_3)^-$ and $(H_7C_3N_6)^+$are 6.34, 3.98, 6.18 eV and 53.45, 126.33, 69.83, respectively. Among them, $(H_2C_3N_3S_3)^-$ exhibits the largest δ and the smallest *E*'. Clearly, this structure-property relationship indicates that as *E*' increases, δ decreases. This makes it impossible to achieve DUV/UV transparent materials with significant birefringence using these three functional groups. Therefore, a key challenge in this research is to rationally modify these groups to increase δ without significantly reducing *E*'.

Previous studies have reported a limited number of cases where the introduction of amino groups (NH_2) onto six-membered rings promotes coplanar arrangements, thereby enhancing optical anisotropy [24–26]. Herein, by applying an amino substitution strategy, our theoretical calculation indicates that $(H_3C_3N_4S_2)^-$ has a high $\delta = 102.26$ with a wide $E' = 4.45$ eV, achieving the best balance among the related six-membered rings (Fig. 1). Subsequently, four new compounds, $A_2(H_3C_3N_4S_2)_2{\cdot}H_2O$ (A=NH_4, **I**; K–Cs, **II**–**IV**) were successfully synthesized. The experimental studies reveal that successful $-NH_2$ substitution makes the optical cutoff edge blue shifts at least 30 nm compared with that of trithiocyanurates [27]. Notably, compound **I** ($E_g = 3.65$ eV, $\Delta n_{cal.}^{max} = 0.510$, $\Delta n_{obv.}^{(0\bar{1}\bar{1})} = 0.413$ at 546 nm) exhibits one of the largest birefringence values among materials with an absorption cutoff edge shorter than 330 nm. The work introduces a new candidate group for preparing optical materials with a desired wide band gap and strong optical anisotropy.

The experimental PXRD patterns align well with the simulated patterns (Fig. S1 in Supporting information), demonstrating the phase purity of the samples at the instrument's detection limit. The chemical compositions of all samples determined by EDS measurements match well with the single crystal diffraction data refinement results (Fig. S2 in Supporting information).

The single-crystal diffraction data of **I**–**IV** are successfully refined and reveal that the unit cells are consisted of two organic anions $[H_3C_3N_4S_2]^-$ (2-amino-4,6-dimercapto-S-triazine), two cations and one crystalline water, giving the formula of $A_2(H_3C_3N_4S_2)_2{\cdot}H_2O$ (Fig. S3 in Supporting information). Compound I crystallizes in monoclinic space group $P2_1/n$, and the others crystallize in triclinic space group $P\bar{1}$ (Tables S1 and S2 in Supporting information, Fig. 2).

The $[H_3C_3N_4S_2]^-$ anions are interconnected by the hydrogen bonds (N–H···S and N–H···N) to form a $[H_3C_3N_4S_2]_\infty$ chain, with NH_4^+ or metal cations are located between the chains (Fig. 2). The N–H···S and N–H···N bond lengths of **I**–**IV** fall in the normal range [28]. Constrained by the centrosymmetric symmetry, the polar anionic units are arranged antiparallel, resulting in an overall dipole moment of zero. (Fig. 2)

As shown in Fig. 2, in compound **I**, each $N(2)H_4^+$ cation is coordinated to two $[H_3C_3N_4S_2]^-$ anions *via* N(2)–H···S (3) = 2.39 Å and N(2)–H···N(3) = 2.07 Å into a dimer. Each dimer was extended *via* N(6)–H···N(7) = 2.13 Å and N(10)–H···N(5) = 2.08 Å into an infinite chain that is further connected *via* N(8)–H···S (2) = 2.47 Å into a 2D layer. The $N(1)H_4^+$ links with one of $[H_3C_3N_4S_2]^-$ unit and utilizes H_2O as medium connect with the $N(2)H_4^+$, forming a *quasi*-2D layer. This *quasi*-2D layer is alternatively stacked along the *b*-axis. In **II**–**IV**, the $[H_3C_3N_4S_2]^-$ anion is connected into an infinite chain *via* the N–H···S = 2.49–2.50 Å, N–H···N = 2.07–2.17 Å, and the metal cation is coordinated to the anion group *via* the S and N forming a 3D structure. The K^+cations are 8-fold coordinated in **II**, the Rb^+ cations are 8-fold and 9-fold coordinated in **III**, and Cs^+ are 9-fold and 10-fold coordinated in **IV**. The K–S bond varies from 3.26 Å to 3.56 Å, and K–N bonds are 2.86 and 2.89 Å and K–O bond is 2.83 Å. In **III**, Rb(1)–S = 3.40–3.59 Å, Rb(1)–N = 3.07–3.55 Å and Rb(1)–O = 2.95 Å to form the 9-fold coordinated polyhedron; and $Rb(2)^+$ is 8-fold coordinated with Rb(2)–S = 3.36–3.69 Å, Rb(2)–N = 2.97 to 3.01 Å and Rb(2)–O = 2.93 Å For **IV**, Cs–S = 3.47–4.11 Å, Cs–N = 3.12–3.82 Å and Cs–O = 3.09–3.19 Å are all falling in the normal bond length range. The bond valence sums (BVS) calculation of K, Rb and Cs atoms are evaluated to be 0.94–1.1, 1.04–1.08 and 1.18–1.21 that is consistent with the expected valance of them.

The thermogravimetric curves of **I**–**IV** indicate that all samples start to decompose at ~380 K (Fig. S4 in Supporting information). In the first stage, **II**–**IV** just release H_2O molecules, but **I** release two NH_3 and one H_2O molecules with the weight loss of 13.69% (calcd. 13.9%) on account of the hydrogen bond interaction weaker than covalent bond. The second and third stage for **I** are attributed to the complex decomposition reaction of the organic group. **II**–**IV** have similar decomposition process in second stage. To check the air and humidity stability, the compounds were placed in a nor-

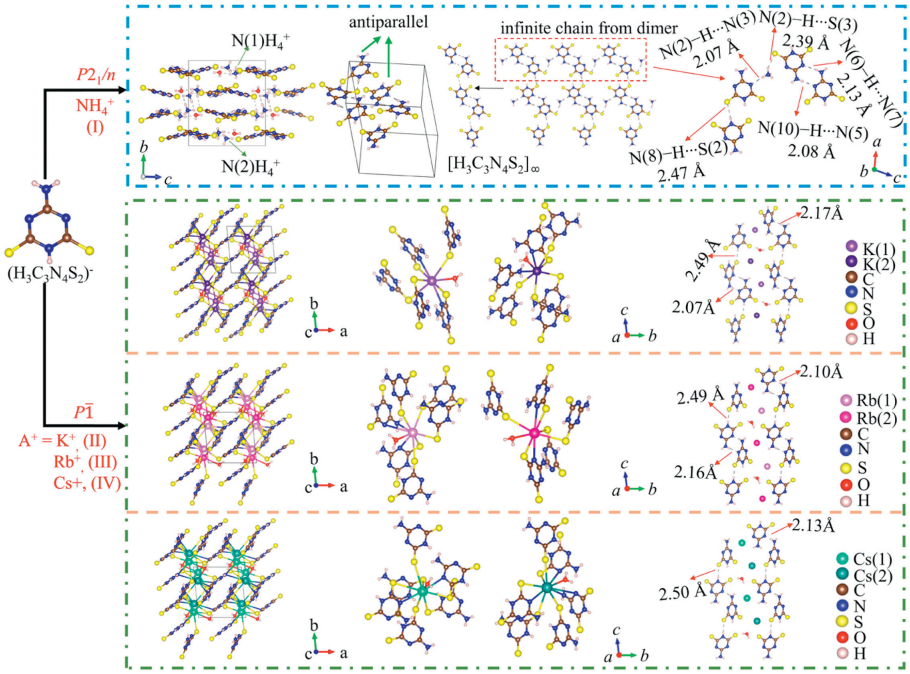


Fig. 2. The structure diagrams and single crystal picture of **I**–**IV**.

mal air environment and the PXRD data were collected again after six months. The results demonstrated that $A_2(H_3C_3N_4S_2)_2{\cdot}H_2O$ (A =NH_4, **I**; K−Cs, **II**–**IV**) show good air stability (Fig. S5 in Supporting information)

The FT-IR spectra of **I**–**IV** show the characteristic vibrations (Fig. S6 in Supporting information). The hydrogen bond related N–H vibrations are found at positions higher than 3500 cm^{-1}. The peak around 3384–3418 cm^{-1} and 1636–1646 cm^{-1} are attributed to the O−H stretching and bending vibrations of H_2O molecule. The hydrogen atom connected with the nitrogen atom on $[H_3C_3N_4S_2]^-$ ring resulting in a N−H stretching vibration at 3113–3124 cm^{-1}. The 1258−1265 cm^{-1} and 771−778 cm^{-1} peaks are assigned to the stretching vibration of C−N and scissor vibration of N−H due to the outside ring NH_2 unit. The C−S and C−N vibrations are located at 1481−1493 cm^{-1}, 863/864 cm^{-1} and 1172−1174 cm^{-1}, 1225−1226 cm^{-1}, respectively. The identification of the $[H_3C_3N_4S_2]$ six-membered ring consists with the results of SC-XRD analysis. Unlike **II**–**IV**, sample **I** exhibit two distinct peaks associated with the stretching and bending vibration of NH^{4+} cation, located at 1404 and 3350 cm^{-1}.

The UV–vis diffuse reflectance spectra of **I**–**IV** reveal an absorption cutoff edge (λ_{cutoff}) of 313 nm for **I**, 317 nm for **II**, 318 nm for **III**, 317 nm for **IV**, respectively (Fig. S7 in Supporting information). The optical band gaps was determined *via* Kubelka-Munk function, $F(R)=(1-R)^2/2R=a/S$, where R is the reflectance, a is the absorption, S is the scattering. Accordingly, the band gaps (E_g) of **I**–**IV** are found to be 3.65, 3.55, 3.52, and 3.53 eV Clearly, the amino substitution strategy (*i.e.*, one S atom of $(H_2C_3N_3S_3)^-$ substituted by $-NH_2$) leads to a significant shift in λ_{cutoff} and E_g when compared to the related $(H_{3-x}C_3N_3S_3)^{x-}$-containing compounds. For example, $Cs(H_2C_3N_3S_3)$ (374 nm, 3.06 eV) [22], $K_2(HC_3N_3S_3){\cdot}1.5H_2O$ (344 nm, 3.36 eV) [23], and $K_2Sr(H_2C_3N_3S_3)_4{\cdot}5H_2O$ (374 nm, 3.04 eV) [27–29]. The band gaps (E_g) of **I**–**IV** are even comparable to the cyanurates, for example, $Pb(H_2C_3N_3O_3)(OH)$ (λ_{cutoff} = 313 nm) [30] and $BaZn_2(H_2C_3N_3O_3)_2(HC_3N_3O_3)(OH)_2{\cdot}2H_2O$ (λ_{cutoff} = 326 nm) [31]. Clearly, the amino group on the six-membered ring significantly reduce the delocalized conjugation between the π-electron system.

The amino group-containing $[H_2C_3N_4S_2]^-$ anion is evaluated to possess exceptional polarizability anisotropy; therefore, the resulting compound $A_2(H_2C_3N_4S_2)_2{\cdot}H_2O$ (**I**–**IV**) is expected to exhibit strong optical anisotropy. According to the crystallographic data, both the monoclinic **I** and the triclinic **II**–**IV** are biaxial crystals that exhibit three principal refractive indices. The correlation between the optical and the crystallographic axes of **I** is illustrated in Fig. 3c, the crystallographic *a*-axis and *c*-axis are 60.3° and 93.9° to the dielectric *x*-axis and *z*-axis, and those of **II**–**IV** are listed in Table S3 (Supporting information). The birefringence of **I**–**IV** were measured under the polarization microscope using Berek compensator (Fig. 3a and Fig. S8 in Supporting information). The retardation (R) values of **I**–**IV** are measured to be 2.480, 10.4, 8.805, and 12.645 μm; and the thickness were measured to be 6, 25, 22, and 30 μm, respectively (Fig. S9 in Supporting information). The crystal orientations of the measured plates were measured using a single crystal diffractometer and found to be $(0\bar{1}\bar{1})$-**I**, $(\bar{1}00)$-**II**, $(\bar{1}00)$-**III**, and (100)-**IV**, respectively (Fig. 3b and Figs. S7d-f). According to the equation $R=\Delta n\times T$, the experimental birefringence at 546 nm of single crystal plates of **I**–**IV** are $\Delta n_{obv.}^{(0\bar{1}\bar{1})}=0.413$, $\Delta n_{obv.}^{(\bar{1}00)}=0.416$, $\Delta n_{obv.}^{(\bar{1}00)}=0.400$ and $\Delta n_{obv.}^{(100)}=0.421$, respectively. The birefringence was calculated with the aid of the first principles theory (Fig. 3d and Figs. S8g-i). These biaxial crystals exhibit three unequal principal refractive indices, with $n_x > n_z > n_y$ for **I**, and $n_z > n_y > n_x$ for II–IV. The maximal birefringence of **I** is calculated to be $\Delta n_{cal.}=n_x - n_y=0.510$@546 nm. This value is larger than most of the cyanurate, $(H_{3-x}C_3N_3O_3)^{x-}$ containing compounds, which range from 0.079 to 0.236 [28]. The calculated $\Delta n_{cal.}$ values of **II**–**IV** are 0.448, 0.445 and 0.440 at 546 nm, respectively (Fig. S8). These value is only slightly lower than that of the trithiocyanurate $(H_{3-x}C_3N_3S_3)^{x-}$ containing compounds, such as $Cs_3Cl(HC_3N_3S_3)$ (0.52@550 nm) [20] and $Cs_2Mg(H_2C_3N_3S_3)_4{\cdot}8H_2O$ (0.58@800 nm) [28]. Moreover, the value is significantly greater than that of commercial birefringence crystals [32–34]. The as-grown plane of **I** as shown in Fig. 3 is $(0\bar{1}\bar{1})$, on which the theoretical maximum birefringence value cannot be observed. Therefore, the as-grown crystal plate **I** reads a value of $\Delta n_{obv.}^{(0\bar{1}\bar{1})}=0.413$. Al-

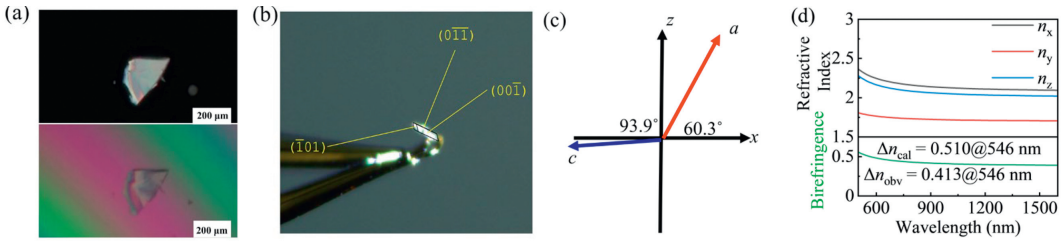


Fig. 3. (a) The crystal plate of **I** observed in cross-polarized light. (b) Crystal orientation of measured plate of **I**. (c) The angles between the crystallographic *a*- and *c*-axis and the optical axes *z* and *x* for **I**. (d) Calculated wavelength-dependent refractive index and birefringence of **I**.

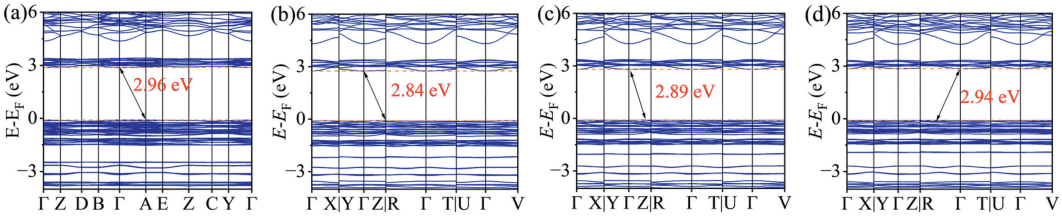


Fig. 4. Band structure of **I** (a), **II** (b), **III** (c) and **IV** (d).

though this is not the highest value, the birefringence is expected to be larger if a properly oriented plate is obtained.

The first-principles calculations were executed to study the correlation between structure and optical characters of **I**–**IV**. The band structures are shown in Fig. 4, revealing the indirect band gaps of 2.96, 2.84, 2.89 and 2.94 eV for **I**–**IV**, respectively. These values imply that the E_g of **I**–**IV** is unaffected by cations; therefore, the valance band maximum (VBM) and conduction band minimum (CBM) are primarily influenced by the anions. The partial density of states (PDOS) and electron localization function (ELF) were analyzed (Figs. S10 and S11 in Supporting information). For **I**–**IV**, the major contributions of VBM are generated from the S 3p and N 2p orbitals, which corresponds to the N–H···S hydrogen bond, and the CBM is mainly composed of C 2p, N 2p and S 3p states indicating the covalent bonds of C–N and C–S within the $[H_3C_3N_4S_2]^-$ anion. According to the electronic structure, the interaction between C, N and S atoms play an important role in determining the optical properties and band gaps of **I**–**IV**; therefore, the band gaps of **I**–**IV** are mainly determined by $[H_3C_3N_4S_2]^-$ anions. The ELFs (Fig. S11) illustrate that alkali metal atoms are surrounded by a spherical distribution of electrons, indicating that they do not contribute to the birefringence of **II**–**IV**. In contrast, the $[H_3C_3N_4S_2]^-$ anions display distinct asymmetric lobes, suggesting that $[H_3C_3N_4S_2]^-$ is the primary contributor to the anisotropy of **I**–**IV** and then influence their birefringence. As shown in Fig. S12 (Supporting information), the dihedral angle between two $[H_3C_3N_4S_2]^-$ six-membered rings is 29.18°, 28.00°, 27.73° and 26.69° of **I**–**IV**, respectively. These data indicate that the coplanarity of the functional $[H_3C_3N_4S_2]^-$ six-membered rings is getting better from **I**–**IV**. Such a trend is confirmed by the structure optimization (Fig. S13 in Supporting information), the optimized dihedral angle decreases from **I**–**IV** (48.15°, 47.80°, 47.67° and 47.53°). According to conventional intuition, better coplanarity is associated with greater anisotropy. Therefore, the compound **I**, which has the poorest coplanarity, should exhibit the smallest birefringence. However, the observed changes in $\Delta n_{obv.}$ and the theoretical calculations of $\Delta n_{cal.}$ show opposite trends. Clearly, factors other than coplanarity play a significant role in determining the magnitude of birefringence of **I**–**IV**. Furthermore, the orientation of the dipole moment of the $[H_3C_3N_4S_2]^-$ anion (*p*) is studied in detail. The *p* in **I** is aligned at an angle of 9.14° from *a*-axis and *p* in **II**–**IV** is aligned at an angle of 11.02°, 11.39° and 11.78° from *c*-axis (Fig. S12). These data indicate that the orientation of the dipole moment of the $[H_3C_3N_4S_2]^-$ anion also influences the birefringence of the compound.

In conclusion, by applying an amino substitution strategy, we report that 2-amino-4,6-dimercapto-*S*-triazine, $(H_3C_3N_4S_2)^-$, can serve as a new DUV/UV active functional structure building unit. Utilizing this building unit, a series new compounds: $A_2(H_2C_3N_4S_2)_2{\cdot}H_2O$ (NH_4, **I**; K-Cs, **II**-**IV**) were discovered. The single crystal structure, optical, and thermal properties are characterized. Compound **I** crystallizes in $P2_1/n$, while compounds **II**-**IV** crystallizes in $P\bar{1}$. Their experimental optical band gaps (E_g) range from 3.52 eV to 3.65 eV, corresponding to a blue shift of 30–60 nm compared to those of the trithiocyanate systems. Moreover, the birefringence of all compounds ranges from 0.440 to 0.510, retaining strong anisotropy. Notably, compound **I** (E_g = 3.65 eV, $\Delta n_{cal.}^{max} = 0.510$, $\Delta n_{obv.}^{(0\bar{1}\bar{1})} = 0.413$@546 nm) exhibits one of the largest birefringence values among organic-inorganic hybrid materials with an absorption cutoff edge shorter than 330 nm. Theoretical calculations confirm the role of the amino substituted-six-membered ring in determining the band gap and birefringence of **I**-**IV**. This work offers a new perspective for designing optical functional groups and developing materials with broad band gaps and strong optical anisotropy.

Declaration of competing interest

The authors declare that they have no known competing financial interests or personal relationships that could have appeared to influence the work reported in this paper.

CRediT authorship contribution statement

Shuang Zhao: Writing – review & editing, Writing – original draft, Formal analysis, Data curation, Conceptualization. **Fei Jia:** Formal analysis, Data curation. **Kaibei Zhan:** Formal analysis, Data curation. **Rui-Xi Wang:** Formal analysis, Data curation. **Pengfei Tan:** Data curation. **Lin Shen:** Data curation. **Li-Ming Wu:** Writing – review & editing, Writing – original draft, Visualization, Validation, Supervision, Formal analysis, Data curation, Conceptualization. **Ling Chen:** Writing – review & editing, Writing – original draft, Supervision, Software, Funding acquisition, Formal analysis, Data curation, Conceptualization.

Acknowledgments

This work was financially supported by the National Natural Science Foundation of China (No. 22193043).

Supplementary materials

Supplementary material associated with this article can be found, in the online version, at doi:10.1016/j.cclet.2024.110625.

References

[1] Q.Q. Liu, X. Liu, L.M. Wu, L. Chen, Angew. Chem. Int. Ed. 61 (2022) e202205587.
[2] L. Xiong, L.M. Wu, L. Chen, Angew. Chem. Int. Ed. 60 (2021) 25063–25067.
[3] Y.Q. Li, X. Zhang, J.Y. Zheng, et al., Angew. Chem. Int. Ed. 62 (2023) e202304498.
[4] L.Q. Yang, X.M. Jiang, Y. Chen, B.W. Liu, G.C. Guo, Adv. Opt. Mater. 12 (2023) 2301897.
[5] W.J. Xie, Z. Fang, J.G. Mao, Inorg. Chem. 61 (2022) 18260–18266.
[6] X.L. Chen, F.F. Zhang, Y.J. Shi, et al., Dalton Trans. 47 (2018) 750–757.
[7] J. Song, C.G. Li, J.M. Jiao, et al., Inorg. Chem. Front. 10 (2023) 5488–5495.
[8] M. Mutailipu, F.M. Li, C.C. Jin, et al., Angew. Chem. Int. Ed. 61 (2022) e202202096.
[9] G. Peng, C.S. Lin, H.X. Fan, et al., Angew. Chem. Int. Ed. 60 (2021) 17415–17418.
[10] L. Qi, X. Jiang, K. Duanmu, et al., Angew. Chem. Int. Ed. 62 (2023) e202309365.
[11] X.F. Wang, Y. Li, Z.L. Chen, et al., Small Struct 4 (2023) 2300274.
[12] Q. Wang, W. Song, Y. Lan, et al., Inorg. Chem. Front. 9 (2022) 3590–3597.
[13] B.L. Cheng, Z.J. Li, Y. Chu, et al., Natl. Sci. Rev. 9 (2022) nwac110.
[14] J.Y. Zuo, Q.Y. Feng, H. Du, Inorg. Chem. 63 (2024) 272–279.
[15] J.Y. Zheng, X.Y. Song, Y.R. Wu, et al., Adv. Funct. Mater. 34 (2024) 2403843.
[16] Y.Q. Li, Q.C. Wu, Z.S. Lin, et al., Fundam. Res. 3 (2023) 974–978.
[17] X.H. Meng, X.Y. Zhang, Q.X. Liu, et al., Angew. Chem. Int. Ed. 62 (2022) e202214848.
[18] D.H. Lin, M. Luo, C.S. Lin, F. Xu, N. Ye, J. Am. Chem. Soc. 141 (2019) 3390–3394.
[19] K.J. Kang, X.H. Meng, F. Liang, et al., Cryst. Eng. Comm. 22 (2020) 2128–2131.
[20] M.J. Li, X. Zhang, Z.Y. Xiong, et al., Angew. Chem. Int. Ed. 61 (2022) e202211151.
[21] Z.Y. Bai, J. Lee, H. Kim, C.L. Hu, K.M. Ok, Small 19 (2023) e2301756.
[22] X. Hao, C.S. Lin, N. Ye, et al., Cryst. Growth Des. 23 (2023) 362–368.
[23] Y.P. Song, W.Q. Huang, Y. Zhou, et al., Cryst. Growth Des. 23 (2023) 1330–1335.
[24] X.G. Du, F.Y. Wang, F. Liang, et al., Inorg. Chem. Front. 10 (2023) 5979–5985.
[25] Y.Q. Li, W.Q. Huang, Y. Zhou, et al., Angew. Chem. Int. Ed. 62 (2022) e202215145.
[26] S.F. Li, L. Hu, Y. Ma, et al., Inorg. Chem. 61 (2022) 10182–10189.
[27] M.J. Li, Z.Y. Wang, B. Ahmed, et al., Chem. Plus. Chem. 88 (2023) e202300094.
[28] X. Hao, C.S. Lin, M. Luo, et al., Inorg. Chem. 62 (2023) 7611–7616.
[29] J.M. Zhao, H.K. Liu, X.D. Zhang, B.B. Zhang, Y. Wang, Cryst. Eng. Comm. 22 (2020) 6495–6501.
[30] Y. Chen, C.L. Hu, Z. Fang, Y.L. Li, J.G. Mao, Inorg. Chem. 61 (2022) 1778–1786.
[31] D.D. Wang, F. Liang, X.Y. Zhang, Z.G. Hu, Y.C. Wu, Cryst. Growth Des. 21 (2021) 2348–2354.
[32] H.T. Luo, T. Tkaczyk, E.L. Dereniak, K. Oka, R. Sampson, Opt. Lett. 31 (2006) 616–618.
[33] D.E. Zelmon, D.L. Small, D. Jundt, J. Opt. Soc. Am. B 14 (1997) 3319–3322.
[34] G.Q. Zhou, J. Xu, X.D. Chen, et al., J. Cryst. 191 (1998) 517–519.